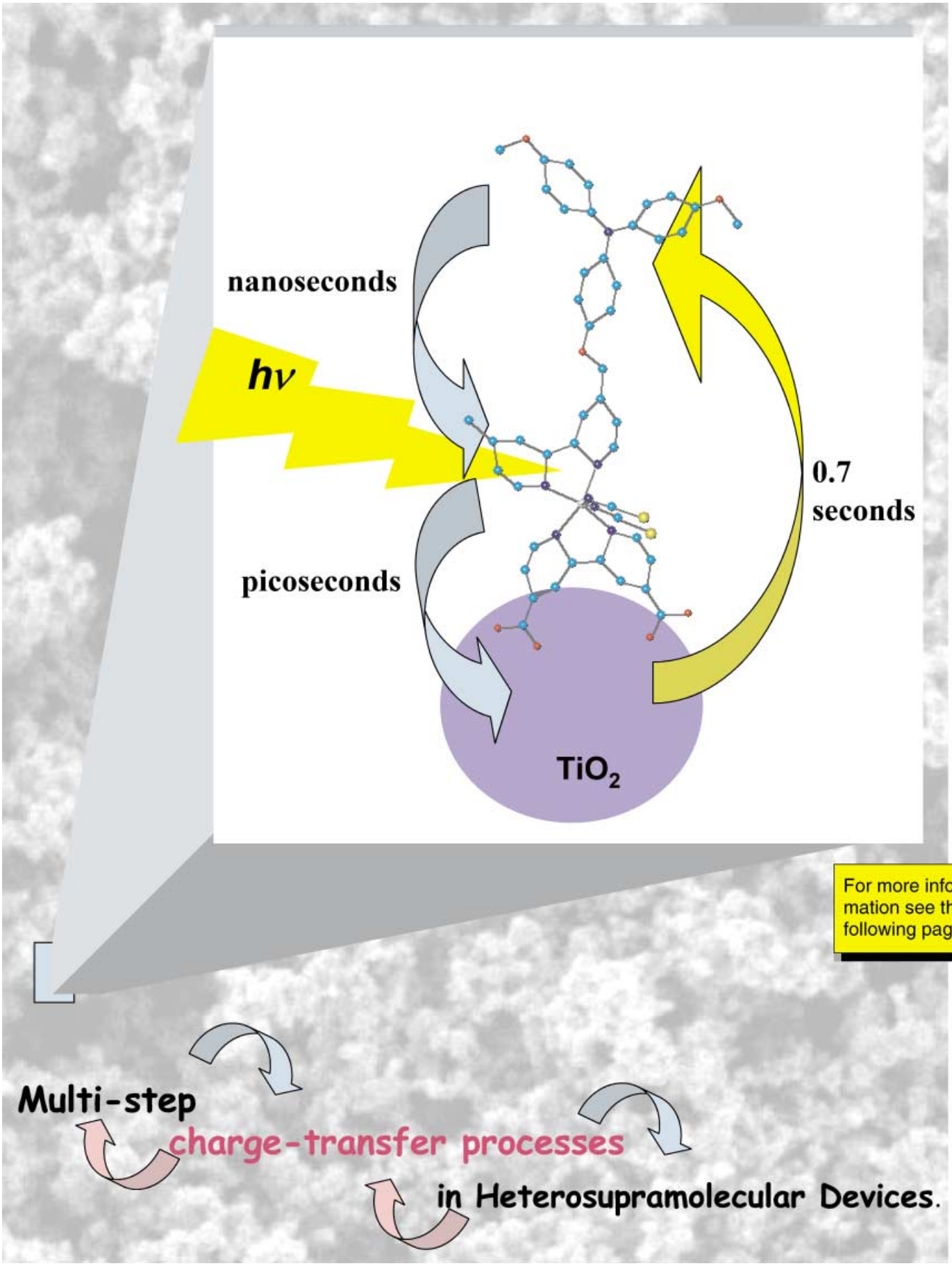

 DOI: 10.1002/chem.200305408

Supramolecular Control of Charge-Transfer Dynamics on Dye-sensitized Nanocrystalline TiO_2 Films

Narukuni Hirata,[a] Jean-Jacques Lagref,[b] Emilio J. Palomares,[a] James R. Durrant,*[a] M. Khaja Nazeeruddin,*[b] Michael Gratzel,[b] and Davide Di Censo[b]

Abstract: A $[Ru(dcbpy)_2(NCS)_2]$ dye has been chemically modified by the addition of a secondary electron donor moiety, *N*,*N*-(di-*p*-anisylamino)phenoxymethyl. Optical excitation of the modified dye adsorbed to nanocrystalline TiO_2 films shows a remarkably long-lived charge-separated state, with a decay half time of 0.7 s. Semiempirical calculations confirm that the HOMO of the modified dye molecule is localised on the electron donor group. The retardation of the recombination dynamics relative to the unmodified control dye is caused by the increase in the spatial separation of the HOMO orbital from the TiO_2 surface. The magnitude of the retardation is shown to be in agreement with that predicted from the non-adiabatic electron-tunnelling theory.

Keywords: dyes/pigments · electron transfer · ruthenium · supramolecular chemistry

Introduction

Light-driven electron-transfer processes between molecular adsorbates, semiconductor nanomaterials and adsorbed redox molecules have been a subject of intense research in recent years.[1] Such electron-transfer processes are fundamental to many applications of semiconductor nanomaterials in photography,[2] photocatalytic degradation of pollutants,[3] quantum dot devices[4] and solar energy conversion.[5] In all of these applications, a key requirement is that light absorption results in the efficient generation of a long-lived charge-separated state. Of particular technological interest are photoelectrochemical solar cells based on dye-sensitised, nanocrystalline, mesoporous TiO_2 films. These molecules have emerged as potential low-cost, effective alternatives to silicon-based devices. Efficient solar cells of this type typically employ **N719** dye (chemical name = bis(2,2′-bipyridyl-4,4′-dicarboxylato)ruthenium(II) bis-tetrabutylammonium sensitiser dye $[(RuL_2(NCS)_2][TBA]_2$ L = 4,4′-dicarboxy-2,2′-bipyridine, TBA = tetrabutylammonium salt), achieving up to 9.18% solar to electric power conversion.[6] It is necessary to achieve high rates of charge separation and collection compared to interfacial charge-recombination processes in order to achieve high device efficiencies. A number of strategies are currently being developed to optimise these dynamics, including the insertion of inorganic barrier layers between TiO_2 and the sensitiser dye,[7] the use of alternative redox couples,[8] and the development of novel sensitiser dyes.[9]On the other hand, the synthesis of supramolecular (multicomponent) molecules is attracting strong interest due to their potential application in molecular electronic devices.[10,11] Such supramolecular structures provide a potentially attractive approach to controlling the charge separation, and recombination dynamics at the molecule/nanocrystal interfaces. In particular, by introducing a secondary electron transfer function, or "supersensitiser" into the supramolecular complex, as illustrated in Scheme 1, it is possible to retard the interfacial charge-recombination dynamics whilst retaining efficient light-induced charge separation. This approach has previously been employed by using either a Ru^{II} tris-bipyridine derivate to demonstrate the supersensitiser function,[12] although the relatively weak red optical absorbance of this dye relative to **N719** precluded its practical device application, or by the use organic molecules such as "molecular spacers" linked to the redox chromophore.[13] In this article, we will provide data showing that by appropriate design of a $[RuL_2(NCS)_2]$ heteroleptic derivate it is possible to achieve molecular control of the back electron-transfer dynamics whilst maintaining good red-light absorption and efficient electron injection. This control is achieved

[a] N. Hirata, Dr. E. J. Palomares, Dr. J. R. Durrant
Imperial College, Department of Chemistry
Centre for Electronic Materials and Devices
Exhibition Road, London SW7 2AY (UK)
E-mail: j.durrant@imperial.ac.uk

[b] Dr. J.-J. Lagref, Dr. M. K. Nazeeruddin, Prof. M. Gratzel, D. Di Censo
Laboratory for Photonics and Interfaces
Institute of Molecular and Biological Chemistry
School of Basic Sciences, Swiss Federal Institute of Technology
1015 Lausanne (Switzerland)
E-mail: MdKhaja.Nazeeruddin@epfl.ch

DOI: 10.1002/chem.200305408

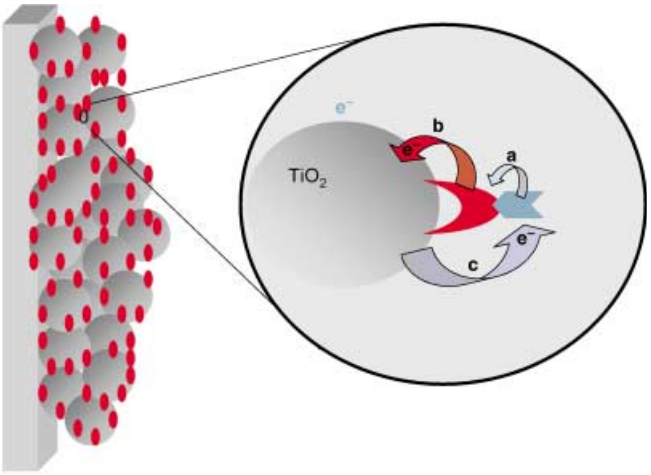

Scheme 1. Schematic representation of electron-transfer (ET) processes in dye-sensitised solar cells showing photogeneration of the dye excited state: a) electron transfer from the secondary electron donor moeity, b) electron injection into the semiconductor and c) the wasteful charge-recombination pathway of the injected electron with the oxidised dye molecules.

by "supersensitising" the dye molecule by the addition of a secondary electron-donor group, in this case *N*,*N*-(di-*p*-anisylamino)phenoxymethyl(DAP) group. This increases the physical separation of the dye cation from the electrode surface and results in remarkably slow, interface limited recombination dynamics.

Results and Discussion

Synthesis and characterisation of [Ru(L)(L′)(NCS)] heteroleptic dye: The details of the synthetic strategy adopted for the preparation of heteroleptic complexes are shown in Scheme 2. During the reaction the intermediate products were drawn off and checked by UV-visible spectroscopy. Reaction of dichloro(*p*-cymene)ruthenium(II) dimer **1** with 4-[4-(*N*,*N*-di-*p*-anisylamino)phenoxymethyl]-4′-methyl-2,2′-bipyridine (L′) in *N*,*N*′-dimethylformamide (DMF) solution at 90 °C resulted in the mononuclear complex **2**, [Ru(L′)Cl(cymene)]Cl. In this step, the coordination of substituted bipyridine ligand to the ruthenium centre takes place with cleavage of the doubly chloride-bridged structure of the dimeric complex.

Heteroleptic dichloro complexes were prepared by reacting the mononuclear complex **2** with 4,4′-dicarboxy-2,2′-bipyridine (L) under reduced light at 150 °C. The displacement of the cymene ligand from the coordination sphere of the ruthenium metal by the 4,4′-dicarboxy-2,2′-bipyridine ligand takes place efficiently in organic solvents such as DMF, without scrambling. The absorption spectra of the resulting complex **3** [Ru(L)(L′)(Cl)$_2$] was measured in ethanol, which

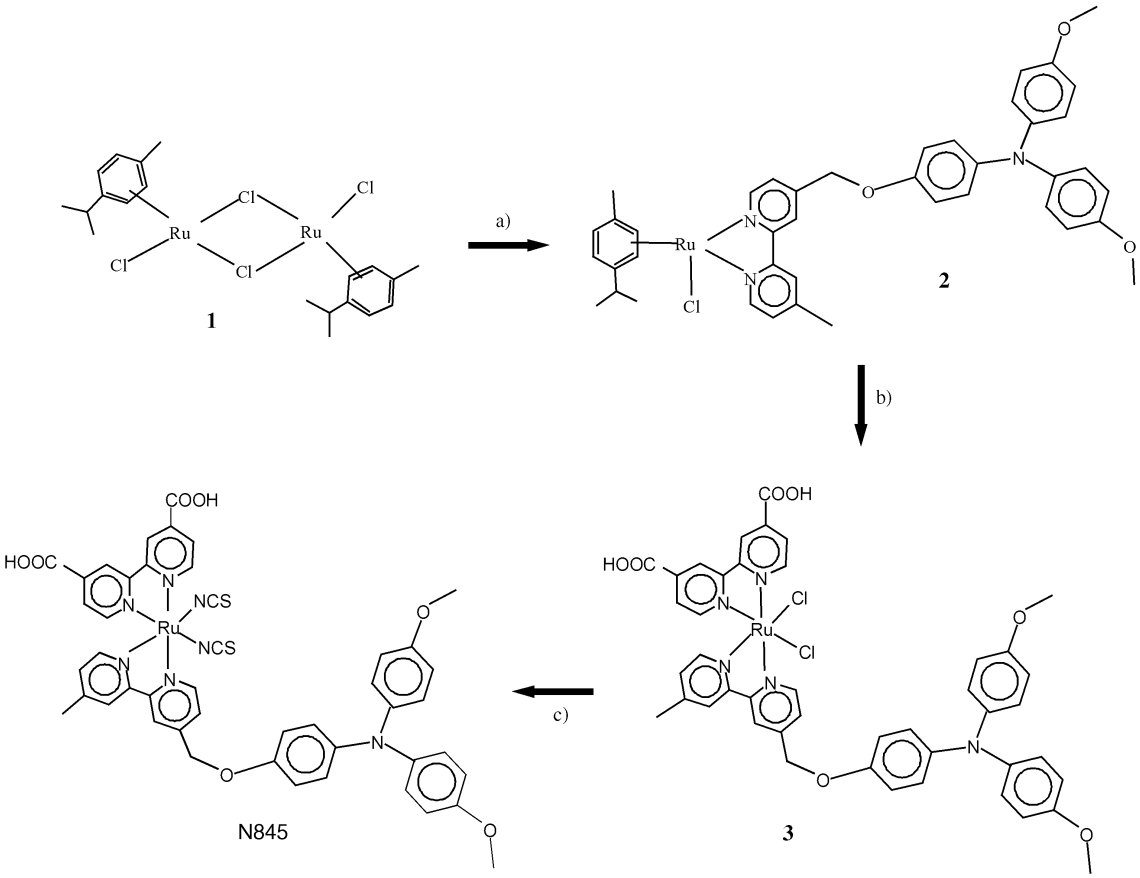

Scheme 2. Schematic of pathways for the synthesis of the **N845** dye: a) 4(4-(*N*,*N*-di-*p*-anisolamino)phenoxymethyl)2,2-bpy, b) DMF, N_2, 4,4′-dicarboxy-2,2′-bpy, c) NH_4NCS, N_2, DMF.

shows bands at 566, 414, 313 and 299 nm. The bands in the visible region at 566 and 414 nm, and in the UV region at 313 and 299 nm, are due to metal-to-ligand charge-transfer transitions (MLCT), and ligand-centered charge-transfer transitions, respectively. The absorption spectra of the $[Ru(L)(L')(Cl)_2]$ complex is identical to that of the complex prepared by means of a $[RuCl_2(DMSO)_4]$ synthetic method.[14] The $[Ru(L)(L')(Cl)_2]$ complex **3** was treated with a 30-fold excess of ammonium thiocyanate ligand to obtain the $[Ru(L)(L')(NCS)_2]$ complex (**N845**). The UV-visible absorption spectra of **N845** show bands at 300, 312, 400, and 535 nm (Figure 1). By comparing with the homoleptic complex **N719**, the UV bands at 299, and 312 nm are assigned to the ligand-centered charge-transfer transitions of the L′, and L ligands, respectively. The absorption spectral data for both complexes are shown in Table 1. When **N845** is excited within the MLCT absorption band at 298 K in an air-equilibrated DMF solution, it exhibits a luminescence maximum at 810 nm. The emission spectral profile is independent of the excitation wavelength. For comparison the **N719** emission spectra is included in Figure 2, which is blue-shifted by 40 nm and the emission intensity is significantly higher than the **N845** complex.

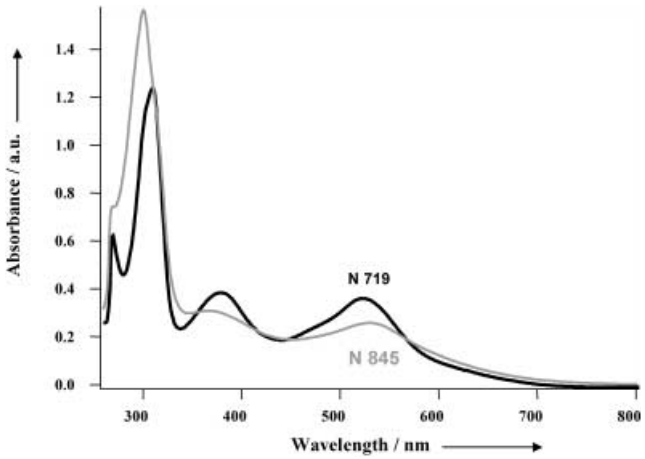

Figure 1. UV/Vis absorption spectra of the complexes **N719** (black line), and **N845** (grey line) in DMF solution.

The ATR-FTIR spectra of **N845** was measured as a solid, and in the adsorbed form onto TiO_2 films. The solid sample of the complex **N845** shows a strong broad band at 1705 cm^{-1} due to carboxylic acid group. The intense peak at 1224 cm^{-1} is assigned to the υ(C–O) stretch. The other characteristic band at 2095 cm^{-1} is assigned to υ(NC) of the thiocyanate ligand. The ATR-FTIR spectra of **N845** adsorbed onto TiO_2 films shows an absence of carboxylic acid bands indicating that the two carboxylic acid groups are dissociated on the surface. The adsorbed dye shows bands at 1611 cm^{-1} ($-COO^-_{as}$), and 1348 cm^{-1} ($-COO^-_{s}$) due to asymmetric (as) and symmetric (s) vibrations of the carboxylate groups, confirming the chelating mode of adsorption between the complex and the TiO_2.

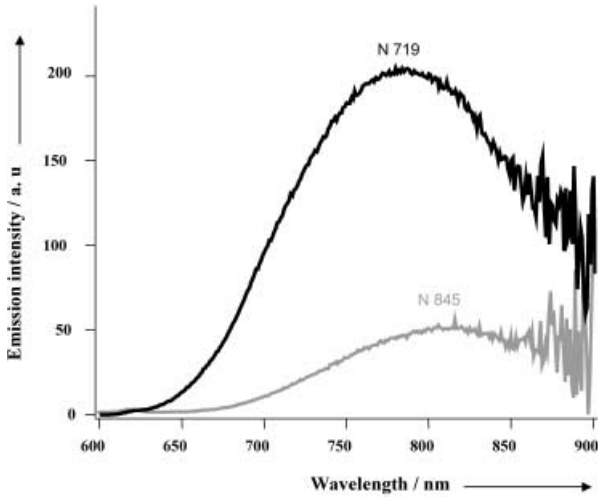

Figure 2. Emission spectra (λ_{ex} = 530 nm) of the complexes **N719** (black line), and **N845** (grey line) at 298 K in DMF.

Semiempirical calculations: For the optimised geometry of the Ru^{II} polypyridyl dyes, we assumed a linkage through the two carboxyl groups (-COOH) to the Ti^{4+} surface, in agreement with the ATR-FTIR data of the adsorbed dye. The semiempirical calculations were performed on the cation state of both dyes.

We first considered the control dye (**N719**). Figure 3 shows a comparison between the optimised geometry of the cation state determined by the semi-empirical ZINDO/1 calculations (see Experimental Methods Section), against the X-ray structure of the fully protonated analogue $[Ru(L)_2(NCS)_2]$ of this dye reported previously.[15] The calculated Ru–N(bpy) and Ru–N(NCS) bond lengths, as summarised in Table 2, are within 1% of those obtained from crystallographic data, supporting the validity of our theoretical calculations. These data also indicate that the removal of one electron from the complexes does not induce dramatic geometric changes. Furthermore these results are in good agreement with DFT calculations reported previously,[15,16] providing further support for the validity of our semiempirical calculations.

Table 1. Absorption and electrochemical properties of the **N845** and **N719** complexes.

Complex	Abs. max. [nm][a] (ε[10^4 м$^{-1}$ cm^{-1}])			$E^{1/2}_{ox}$ [V vs Fc][b]	$E^{1/2}_{ox}$ [V vs. Fc]	$E^{1/2}_{red}$ [V vs. Fc]	$E^{1/2}_{red}$ [V vs. Fc]
	L′(π–π*)	L(π–π*)	4d–π*	L′$^+$/L′	$Ru^{III/II}$	L/L$^-$	L′/L′$^{-1}$
N845	300(5.52)	312 (4.41)	372 (1.05), 535 (1.1)	0.200	0.34	−2.13	−2.40
N719	–	312 (4.91)	396 (1.43), 535 (1.47)	–	0.35(irr)	−2.21	–

[a] λ max and ε values are ±2 nm and ±10%, respectively. [b] The ferrocene/ferrocinium complex used as a reference, which is +640 mV vs SHE.

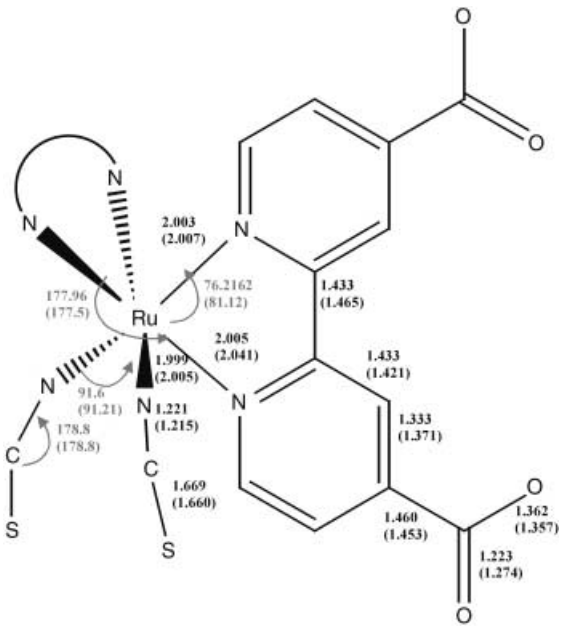

Figure 3. Comparison of bond (black) distances and angles (grey) calculated using ZINDO/1 for the cation state of **N719** with the corresponding experimental X-ray data.[27] The values in parentheses correspond to the X-ray data.

Table 2. Comparison of bond lengths [Å] and angles [°] of crystallographic data for *cis*-[Ru(L)$_2$(NCS)$_2$] with ZINDO/1-optimised geometries for the cation states of **N719** and **N845**.

	cis-[Ru(L)$_2$(NCS)$_2$][c]	**N719**[d]	**N845**[d]
Ru–-NCS	2.025	1.999	1.97
Ru–N(bpy)	2.065	2.042	1.99
NCS-Ru-NCS[a]	91.9	91.6	87.56
N(bpy)-Ru-N(bpy)	81.3	76.21	75.98
(bpy)-(bpy)[b]	90.6	89.98	87.58

[a] NCS-Ru-NCS refers to the bpy ligands *cis* to the NCS ligands. [b] Dihedral angle between the mean planes of bipyridine ligands. [c] Crystallographic data from ref. [27]. [d] Data from semiempirical calculations.

The important distances and angles for the optimised geometries of both dyes, **N719** and **N845**, in their cation states obtained from the ZINDO/1 calculations are compared in Table 2. These data show that the Ru metal co-ordination centres of both dyes are expected to be very similar, as seen by the close match of their optical absorbance spectra as detailed in Table 1. The orbital profiles for the HOMO's of both dyes are presented in Figure 4. The HOMO of the **N719** has a larger amplitude on NCS ligands, (similar results were obtained by Rensmo et al.)[17] and within the NCS ligands the amplitude is more on the sulfur atom. The HOMO for the **N845** is shifted to the secondary electron donor moiety, displacing the positive charge (hole) in the oxidised form of **N845** from the NCS ligands closer to the triphenyl amine group. This results in an increased separation of the HOMO orbital from the TiO_2 surface, as desired in order to achieve slower charge-recombination dynamics.

Electrochemistry: Cyclic voltammetry was used to investigate the electrochemistry of the **N719** and **N845** dyes. Midpoint potentials of these data are summarised in Table 1.

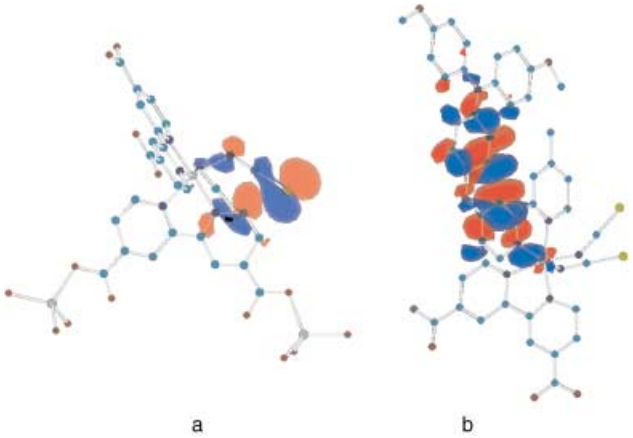

Figure 4. Graphical representation of the HOMOs of a) **N719** and b) **N845** complexes. Atoms in turquoise, red, blue and pale yellow correspond to carbon, oxygen, nitrogen and sulfur, respectively.

Cyclic voltammograms of the complex **N845** in DMF revealed two reversible, one-electron oxidation processes at $E_{1/2} = 0.200$ and 0.34 V versus ferrocene/ferrocinium couple (Fc/Fc^+). The 0.34 V couple, which is also observed for the **N719** control dye, is assigned to the $Ru^{II}/^{III}$ couple. The 0.20 V couple is therefore assigned to the oxidation of donor N,N-(di-*p*-anisylamino)phenoxymethyl group, consistent with the electron donating function of this group. In addition, two quasi-reversible reduction peaks are observed for **N845** at −2.13 and −2.4 V versus Fc/Fc^+. Comparison with the reduction peak observed for the control **N719** dye allows us to assign these reduction peaks for **N845** to the reduction of L and L′ ligands, respectively. These data therefore indicate that the LUMO of the L′ ligand is higher than that of the L ligand. Optical excitation of the **N845** MLCT state is therefore expected to result in electron localisation on the 4,4′-dicarboxy-2,2′-bipyridine (L) ligand, thereby favouring efficient electron injection into the TiO_2 electrode.

Transient absorption and luminescence measurements: The primary function of the *N*,*N*-(di-*p*-anisylamino)phenoxymethyl (DAP) group is to accept the positive charge (hole) after electron injection from the dye-excited state into the conduction band of the nanocrystalline TiO_2. This results in an increase in the physical separation of the charged species. To assay this function, we employed transient absorption spectroscopy to measure the charge-recombination kinetics (reaction c, Scheme 1). The decay of the induced absorption of the **N719** and **N845** cations was monitored following pulsed laser excitation of the dye-sensitised TiO_2 films, in the absence of any applied bias or redox-active electrolyte. Typical data for the charge-recombination process is shown in Figure 5. It is apparent that the decay dynamics of the **N845** dye cation are retarded 1000-fold relative to that of the **N719** cation, with decay half times, $t_{50\%}$, of 0.71 s and 0.85 ms, respectively. This retardation cannot be attributed to differences in oxidation potential of the two dyes, as the recombination reaction is thought to occur in the Marcus "inverted region".[18] This is where the smaller reaction free energy of the **N845** dye would be excepted to result in accel-

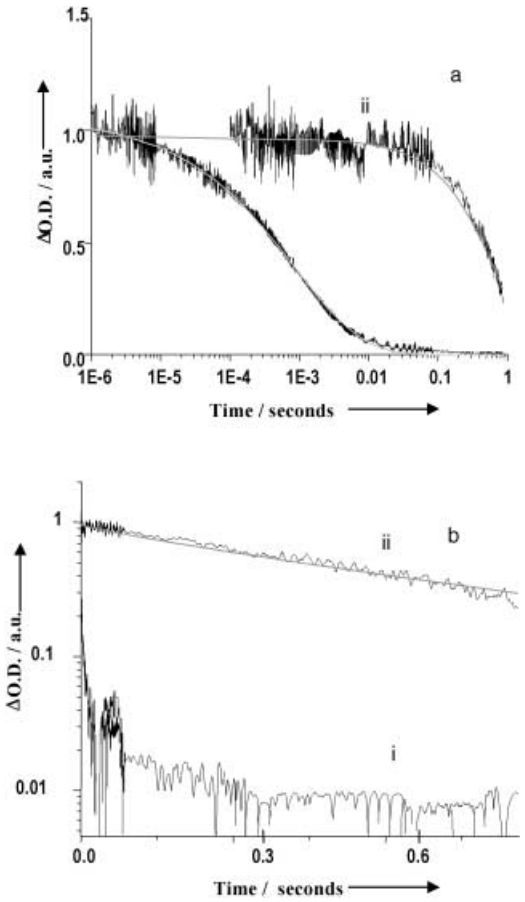

Figure 5. Transient absorption data monitoring charge-recombination dynamics for TiO_2 films sensitised with i) **N719** and ii) **N845**. Both figures show the same data with a) being a linear/log plot and b) being log/linear plot. The grey lines are the fits to the decay kinetics corresponding to i) a streched exponential ($\Delta O.D. \propto \exp(-(t/\tau)^{\alpha})$, $\alpha = 0.44$) and ii) a monoexponenetial decay. The signal size has been normalised for comparisson purposes. Data collected at a probe wavelength of 800 nm for **N719** and 850 nm for **N845**, following optical excitation at 550 nm.

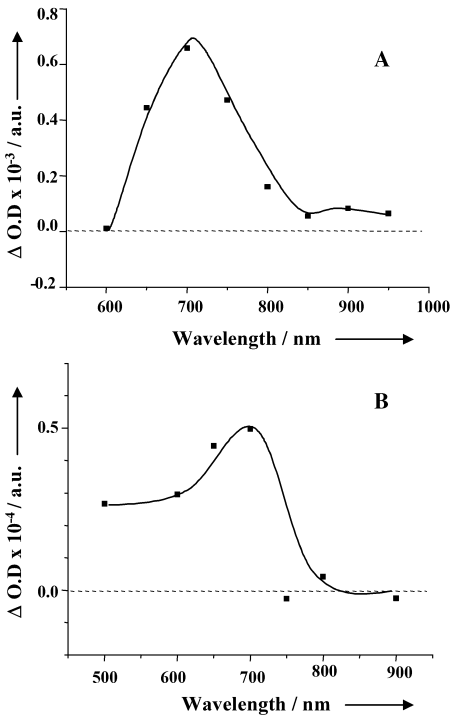

Figure 6. A) Transient absorption specta for TiO_2 films sensitised with **N845** monitored at 8 μs after excitation at 516 nm and B) transient absorption of 4-(diphenylmaino) benzaldehyde (optical absorbance $\lambda_{410\,nm} = 0.35$) monitored at 8 μs after excitation at 400 nm.

erated recombination dynamics, contrary to the experimental observation. Instead the retardation is attributed to an increased distance of the dye cation from the electrode surface due to localisation of the **N845** cation on the DAP moiety, consistent with the semiempirical calculations and electrochemical data detailed above.

Localisation of the **N845** dye cation on the DAP moiety is further supported by the transient absorption spectrum of the dye cation. Figure 6 compares the transient absorption spectrum of the **N845** dye cation generated following photoexcitation of the **N845** dye adsorbed to the TiO_2 electrode (Figure 6a) with the transient spectrum observed for the 4-(diphenylamino) benzaldehyde, closely analogous to the DAP moiety alone (see inset to Figure 6b), adsorbed directly to the electrode (Figure 6b). In both cases, a photoinduced absorption maximum is observed at ~700 nm, assigned to an absorption maximum of the DAP cation, consistent with previous observations,[19] and confirming the localisation of the **N845** cation on the DAP moiety. We note that in the case of Figure 6b, the photoinduced absorption exhibits rapid kinetics (8 μs), consistent with the expected small spatial separation of this cation from the electrode surface.

The initial amplitudes of the dye cation transient absorption signals observed for both the **N845** and **N719** sensitised TiO_2 were of similar magnitudes (ΔODs of 1.4 at 700 nm and 1 at 800 nm, respectively). This observation strongly suggests that, as for **N719**, the optical excitation of the **N845** adsorbed to the TiO_2 films results in efficient electron injection into TiO_2 conduction band. However, uncertainty over the **N845** cation extinction coefficient prevents quantitative analysis from these data alone. Transient luminescence studies, as shown in Figure 7, further indicate efficient electron

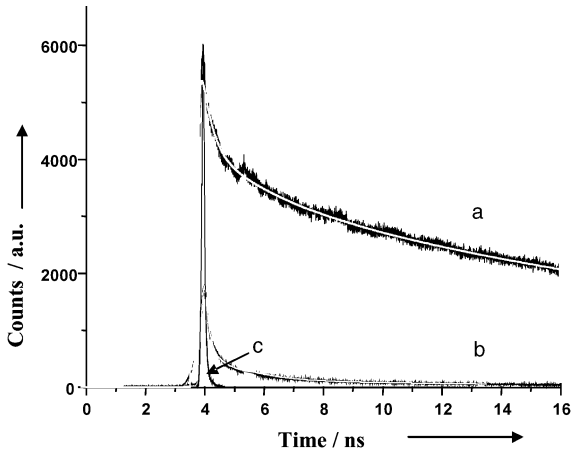

Figure 7. Time-resolved single-photon-counting decays of emission from **N845** sensitised on a) ZrO_2 and b) TiO_2; c) corresponds to the instrument response pulse.

injection for the **N845** sensitised TiO_2 films. These comparisons show the transient luminescence decay of **N845** sensitised TiO_2 and ZrO_2 films, normalised to the same number of absorbed photons. ZrO_2 film was employed as a control film, as the relatively high conduction band edge of this material prevents electron injection, consistent with the long excited state lifetime observed for dyes adsorbed to this film.[20] It is apparent that relative to the control ZrO_2 films, the **N845** luminescence is strongly quenched on the TiO_2 film, consistent with efficient electron injection.

Electron transfer dynamics typically exhibit an exponential dependence upon spatial separation.[Eq. (1)]

$$k_{et} \propto e^{-\beta r} \quad (1)$$

In which **r** is the edge-to-edge separation of the donor and acceptor wave-functions, and β is a measure of the barrier height of the intervening medium. Typically β varies from 2.8 $Å^{-1}$ for a vacuum to 1 $Å^{-1}$ for saturated-electron-orbital densities. From consideration of the HOMO orbital distributions shown in Figure 4, we estimate the dye-cation/electrode-surface distance is increased by 4 Å for **N845** relative to **N719**. Comparison with the ~1000 fold retardation of the observed recombination dynamics yields a value for β of 1.6 $\pm$ 0.2 $Å^{-1}$, typical of β values observed for through solvent electron transfer.[21] It can thus be concluded that the retardation of the recombination dynamics shown in Figure 5 is in good quantitative agreement with that expected from the increased dye-cation/electrode separation determined from the HOMO orbital calculations.

In addition to the retardation of the recombination dynamics shown in Figure 5, it is apparent that the temporal recombination shape differs significantly between these two dyes. For dye **N719**, decay kinetics strongly suggest a stretched exponential (ΔO.D. ~$\exp(-(t/\tau)^{\alpha})$; $\alpha = 0.44$). Such stretched exponential recombination dynamics are typical of those we have observed previously for a range of different dyes under similar experimental conditions. In contrast, for dye **N845** the recombination dynamics suggests an excellent fit to a near monoexponential decay (ΔO.D. ~$\exp(-(t/\tau)^{\alpha}$; α ~0.9) as illustrated by the log/linear plot shown in Figure 5b.

We have previously demonstrated that the stretched exponential recombination dynamics, as observed here for the nanocrystalline TiO_2 films sensitised by **N719**, are consistent with the charge-recombination dynamics being rate limited by electron transport within the metal oxide film.[22] The stretched exponential nature of these kinetics have been attributed to an inhomogeneous distribution of trap depths in the film, resulting in a broad distribution of detrapping (and therefore recombination) times. Our observation that **N845** exhibits recombination dynamics three orders of magnitude slower than **N719** in itself suggests that for this sensitiser, interfacial electron transfer is critical to determining the overall recombination dynamics. The near monoexponential behaviour is indicative of the recombination dynamics being limited by the interfacial electron dynamics, as we have discussed previously in relation to experimental data obtained with two porphyrin dyes.

It can be concluded that this heterosupramolecular approach translates the oxidising equivalent (hole) away from the nanostructured semiconducting surface. The increase in the distance between the surface and the hole, results in an extremely long-lived charge-separated pair. The *N*,*N*-(di-*p*-anisylamino)phenoxymethyl secondary electron-donor group employed in this study can be expected to interface well with triarylamine-based hole conductors, making this sensitiser dye particularly attractive for applications in solid state dye-sensitised solar cells.

Experimental Section

Materials: The dichloro(*p*-cymene)ruthenium(II) dimer and potassium thiocyanate were obtained from Aldrich and used as received. The 4-(diphenylamino)benzaldehyde was purchased from Fluka. The HPLC grade solvents from Fluka were used without purification. 4,4′-Dimethyl-2,2′-bipyridine ligand (from Fluka) was dried under vacuum (9 mbar) at 40 °C for 4 h before use. Water content was measured by Karl-Fisher automatic titration using the coulometer Metrohm 684 KF. Silicagel 60 from Fluka was used for chromatography as a stationary phase. Tris(*p*-anisyl)amine and 4-(*N*,*N*-di-*p*-anisylamino)phenol were synthesised by using the procedure developed by Bonhôte et al.[23]

The preparation of anatase nanocrystalline TiO_2 films (average particle diameter: 15 nm and film thickness 4 μm) and sensitisation of these films were conducted as described previously.[24]

Electrochemistry experiments: Electrochemical data were obtained by cyclic voltammetry using a three-electrode cell and an Auto lab System (PGSTAT 30, GPES 4.8 software). The working electrode was a 0.03 cm^2 gold disk, the auxiliary electrode was a glassy carbon rod and a silver wire was used as quasi-reference electrode. Tetrabutyl ammonium perchlorate (TBAP) 0.1 M was used as supporting electrolyte in DMF. Ferrocene was added to each sample solution at the end of the experiments and the ferrocenium/ferrocene redox couple was used as an internal potential reference.

Spectroscopy: UV/VIS and fluorescence spectra were recorded in a 1 cm pathlength quartz cell on a Cary 5 spectrophotometer and Spex Fluorolog 112 Spectroflurimeter, respectively. The details of the transient absorption spectrometer system for measuring the charge-recombination dynamics are given elsewhere.[25] Transient absorption data were collected with the films covered in ethylene carbonate/propylene carbonate 50:50 v/v. The excitation wavelength was 550 nm for both dyes (20 μJ). The dye volume loaded was selected to achieve matched optical densities of 0.8 absorption units at this wavelength.

Transient emission data were collected using a 635 nm excitation from a IBH NanoLED-06 pulsed laser diode [repetition rate one-shot to 1 MHz, pulse duration (1.3 ns), intensity (~1 mW)]. Emission was collected at 750 nm (bandwidth 50 nm) at a microchannel plate, with an instrument response of 350 ps. Data were collected at matched data collection times of 2500 s.

^1H and ^{13}C NMR spectra were measured with a Bruker ACP-200 spectrometer at 200 MHz and 50.3 MHz, respectively. The reported chemical shifts were against TMS. FAB-MS spectra were obtained at the University of Lausanne from a nitrobenzyl alcohol matrix. The ATR-FTIR spectra for all the samples were measured using a Digilab 7000 FTIR spectrometer. The FTIR data reported here were taken with the "Golden Gate" diamond anvil ATR accessory (Graseby-Specac) using typically 64 scans at a resolution of 2 cm^{-1}. The samples were all measured under the same mechanical force pushing the samples in contact with the diamond window. No ATR correction was applied to the data.

Synthesis and characterisation4-(Bromomethyl)-4′-methyl-2,2′-bipyridine (L): This ligand was synthesised with a slight modification of Meyer's procedure.[26] In a 100 mL round-bottomed flask 4,4′-dimethyl-2,2′-bipyridine (1.8 g, 9.78 mmol), *N*-Bromosuccinimide (1.8 g, 10.1 mmol) and azobis(isobutyronitrile) (50 mg) were added to freshly distilled CCl_4 (40 mL). The mixture was stirred magnetically and heated to reflux for

3 h in the dark. The mixture was cooled to room temperature and the resulting white precipitate filtered using a crucible. The filtrate was evaporated under vacuum and dissolved in CH_2Cl_2 (10 mL) . Silica was added to the solution and then the solvent was evaporated. The SiO_2 with adsorbed product was charged onto a chromatography column (internal diameter 15 mm, length 300 mm) containing silica, which was pre-treated with CH_2Cl_2/NH_4OH 99.5:0.5.4-(Bromomethyl)-4′-methyl-2,2′-bipyridine was obtained by eluting with CH_2Cl_2/hexane 80:20 solvent mixture. The solution was evaporated under vacuum and a yellowish sticky oil was obtained at a yield of 40%. ^{1}H NMR ($CDCl_3$, 298 K):$\delta =$ 2.46 (s, 3H), 4.50 (s, 2H), 7.16 (dd, J=4.4 Hz, 1H), 7.34 (dd, J=4 Hz, 1H), 8.25 (d, J= 1.6 Hz, 1H), 8.43 (d, J=1 Hz, 1H), 8.56 (d, J=5 Hz, 1H), 8.68 ppm (d, J=5.4 Hz, 1H).

4-[4-(*N*,*N*-Di-*p*-anisylamino)phenoxymethyl]-4′-methyl-2,2′-bipyridine (L′): In a dry 25 mL round bottom flask, under argon and at 293 K, 4-(*N*,*N*-di-*p*-anisylamino)phenol (294 mg, 1.2 equiv, 0.91 mmol) and potassium *tert*-butoxide (114 mg, 1.5 equiv, 1.18 mmol) were mixed with dry THF (6 mL). The mixture was magnetically stirred for 20 min, which rapidly turned green. Then, 4-(bromomethyl)-4′-methyl-2,2′-bipyridine (200 mg, 0.76 mmol) was dissolved in dry THF (8 mL) and added with a syringe. A white precipitate of KBr formed progressively. After 35 h the reaction was quenched with water (1 mL). The solvent was removed in a rota-evaporator and tert-butyl methyl ether (TBME) (50 mL) and water (40 mL) was added. The vial was shaken, and the organic phase was allowed to separate. The aqueous phase was washed twice with TBME (20 mL). The collected organic phase was evaporated under vacuum to afford a yellow-green oil. The waxy solid was purified by chromatography (SiO_2, solid deposition, internal diameter 13 mm, high 200 mm) with silica gel previously treated with hexane/triethylamine 99:1. A linear evolution of the eluent composition (over a volume of 250 mL) from pure hexane to hexane/*tert*-butyl methyl ether 50:50 was used. Fractions containing the desired product were evaporated under vacuum to afford a colourless oil, which was dissolved in DMF under argon and kept at 0°C to avoid oxidation by air. Air oxidation was characterised by a strong purple colour. Yield = 200 mg, 52%. ^{1}H NMR ($CDCl_3$, 298 K, 200 MHz):$\delta =$ 2.46 (s, 3H), 3.79 (s, 6H), 5.14 (s, 2H), 6.77–7.01 (m, 12H), 7.12 (d, J=7.6 Hz, 1H), 7.48 (d, J=3.8 Hz, 1H), 8.26 (s, 1H), 8.44 (s, 1H), 8.56 (d, J=5.03 Hz, 1H), 8.70 (d, J=5.05 Hz, 1H); ^{13}C NMR ($CDCl_3$, 298 K): δ=21.2, 55.4, 68.8, 114.53, 115.5, 119.1, 121.6, 122.2, 124.2, 124.9, 125.1, 134.0, 148.5, 149.4, 154.9, 155.0 ppm; Mass spectra (FAB): calcd 503.59, measured 504.6 [MH$^+$] (100%).

Synthesis of [Ru(L)(L′)(NCS)$_2$] (3): [{RuCl(*p*-cymene)]$_2$](0.115 g, 0.188 mmol) was dissolved in DMF (30 mL)and L′(0.19 g, 0.376 mmol)-was added. The reaction mixture was heated at 80°C under nitrogen for 4 h and then, L(0.0917 g, 0.376 mmol)was added . The reaction mixture was refluxed at 160°C for another 4 h under reduced light to avoid light-induced *cis* to *trans* isomerisation. Then an excess of NH_4NCS (13 mmol) was added to the reaction mixture and heated at 130°C for a further 5 h. The solvent was removed using a rotary-evaporator under vacuum. Water was added to the resulting semisolid to remove excess NH_4NCS. The water-insoluble product was collected on a sintered glass crucible by suction filtration and washed with distilled water, followed by diethyl ether and dried. The crude complex was dissolved in a solution of tetrabutyl ammonium hydroxide (0.4 g) in methanol (4 mL). The concentrated solution was charged onto a Sephadex LH-20 (2×30 cm) column and eluted with methanol. The main red band was collected and concentrated to 3 mL. The required complex was isolated upon addition of a few drops of 0.01 M HNO_3. Yield = 0.18 g, 50%. ^{1}H NMR ([D$_4$]CD_3OD, 200 MHz): δ=2.78 (s, 3H), 3.79 (s, 6H), 5.42 (s, 2H), 6.79–7.03 (m), 7.38 (d, 1H), 7.65 (d, 1H), 7.82 (d, 1H), 7.85 (d, 1H), 7.96 (d, 1H), 8.3 (d, 1H). 8.38 (s, 1H), 8.5 (s, 1H), 8.89 (s, 1H), 9.02 (s, 1H), 9.51 (d, 1H), 9.54 ppm (d, 1H).

Semiempirical chemical calculations: Molecular orbitals and optimised geometries for free molecules were calculated using Hyperchem 7 program package running on a PC AMD Athlon® XP-2000+ 1.25 GHz. Geometrical optimisations were performed with the ZINDO/1 parameter set. The overlap weighting factors σ–σ and π–π were set at 1.265 and 0.585, respectively. The number of singly excited configurations used was 1250 (25×25 occupied×virtual orbitals).

Acknowledgement

We gratefully acknowledge the financial support from the EPSRC, the European Union (Contract Number: ENK6-CT-2001–00560 Nanomax), the Swiss Federal Office for Energy (OFEN) and US Air Force Research Office under contract number F61775–00-C0003. E.P. is very grateful for the support of a Marie Curie Fellowship and N.H. for the support of the Bridgestone Corporation. Supply of the **N719** dye from Johnson Matthey is also gratefully acknowledged.

[1] C. A. Koval, J. N. Howard, *Chem. Rev.* **1992**, *92*, 411.
[2] I. R. Gould, J. R. Lenhard, A. A. Muenter, S. A. Godleski, S. Farid, *Pure Appl. Chem.* **2001**, *73*, 455.
[3] M. A. Fox, M. T. Dulay, *Chem. Rev.* **1993**, *93*, 341.
[4] A. Meier, D. C. Selmarten, K. Siemoneit, B. B. Smith, A. J. Nozik, *J. Phys. Chem. B* **1999**, *103*, 2122.
[5] B. O'Reagan, M. Gratzel, *Nature* **1991**, *353*, 737.
[6] M. K. Nazeeruddin, R. Splivallo, P. Liska, P. Comte, M. Gratzel, *Chem. Commun.* **2003**, 1456.
[7] E. Palomares, J. N. Clifford, S. A. Haque, T. Lutz, J. R. Durrant, *J. Am. Chem. Soc.* **2003**, *125*, 475.
[8] H. Nusbaumer, J.-E. Moser, S. M. Zakeeruddin, M. K. Nazeeruddin, M. Graetzel, *J. Phys. Chem. B* **2001**, *105*, 10461.
[9] M. Yanagida, A. Islam, Y. Tachibana, G. Fujihashi, R. Katoh, H. Sugihara, H. Arakawa, *New J. Chem.* **2002**, *26*, 963.
[10] X. Marguerettaz, D. Fitzmaurice, *J. Am. Chem. Soc.* **1994**, *116*, 5017.
[11] X. Marguerettaz, R. O'Neill, D. Fitzmaurice, *J. Am. Chem. Soc.* **1994**, *116*, 2629.
[12] R. Argazzi, C. A. Bignozzi, T. A. Heimer, F. N. Castellano, G. J. Meyer, *J. Am. Chem. Soc.* **1995**, *117*, 11815.
[13] P. G. Hoertz, R. A. Carlisle, G. J. Meyer, D. Wang, P. Piotrowiak, E. Galoppini, *Nano Lett.* **2003**, *3*, 325.
[14] S. M. Zakeeruddin, M. K. Nazeeruddin, R. Humphry-Baker, P. Pechy, P. Quagliotto, C. Barolo, G. Viscardi, M. Gratzel, *Langmuir* **2002**, *18*, 952.
[15] K. Srikanth, V. R. Marathe, M. K. Mishra, *Int. J. Quantum. Chem.* **2002**, *89*, 535.
[16] M. K. Nazeeruddin, S. M. Zakeeruddin, R. Humphry-Baker, S. I. Gorelsky, A. B. P. Lever, M. Gratzel, *Coord. Chem. Rev.* **2000**, *208*, 213.
[17] H. Rensmo, S. Lunell, H. Siegbahn, *J. Photochem. Photobiol. A* **1998**, *144*, 117.
[18] S. Fukuzumi, *Org. Biomol. Chem.* **2003**, *1*, 609.
[19] A. C. Bhasikuttan, A. K. Singh, D. K. Palit, A. V. Sapre, J. P. Mittal, *J. Phys. Chem. A* **1999**, *103*, 4703.
[20] Y. Tachibana, J.-E. Moser, M. Graetzel, D. R. Klug, J. R. Durrant, *J. Phys. Chem.* **1996**, *100*, 20056.
[21] D. S. Bendall, *Protein Electron Transfer*, BIOS Scientific, Oxford, **1996**.
[22] J. N. Clifford, G. Yahioglu, L. R. Milgrom, J. R. Durrant, *Chem. Commun.* **2002**, 126.
[23] P. Bonhote, J.-E. Moser, R. Humphry-Baker, N. Vlachopoulos, S. M. Zakeeruddin, L. Walder, M. Gratzel, *J. Am. Chem. Soc.* **1999**, *121*, 1324.
[24] Y. Tachibana, S. A. Haque, I. P. Mercer, J. R. Durrant, D. R. Klug, *J. Phys. Chem. B* **2000**, *104*, 538.
[25] S. A. Haque, Y. Tachibana, D. R. Klug, J. R. Durrant, *J. Phys. Chem. B* **1998**, *102*, 1745.
[26] S. Gould, G. F. Strouse, T. J. Meyer, B. P. Sullivan, *Inorg. Chem.* **1991**, *30*, 2942.
[27] V. Shklover, Y. E. Ovchinnikov, L. S. Bragnisky, S. M. Zakeeruddin, M. Graetzel, *Chem. Mater.* **1998**, *10*, 2533.

Received: July 29, 2003
Revised: October 16, 2003 [F5408]